ELSEVIER

Journal of Nuclear Materials 278 (2000) 111–116

journal of nuclear materials

www.elsevier.nl/locate/jnucmat

Interpretation of the impurity distribution in the divertor during divertor plate biasing using the DIVIMP code ☆

E. Haddad [a,b,*], F. Meo [a,c], R. Marchand [a,c], G. Ratel [a,d], B.L. Stansfield [a,c], J. Gunn [a,b], P.C. Stangeby [a,e], J.D. Elder [a,e], S. Lisgo [a,e], K. Krieger [a,f]

[a] *Centre canadien de fusion magnétique, 1804 Boulevard Lionel-Boulet, Varennes, Québec, J3X 1S1, Canada*
[b] *MPB Technologies Inc., Dorval, Québec, Canada*
[c] *INRS-Énergie et Matériaux, Varennes, Québec, Canada*
[d] *Hydro-Québec, Varennes, Québec, Canada*
[e] *University of Toronto, Ontario, Canada*
[f] *Max-Plank-Institut für Plasmaphysik, Garching, Germany*

Received 15 August 1998; accepted 15 July 1999

Abstract

Simulations of carbon transport using the DIVIMP code [P.C. Stangeby, J.D. Elder, J. Nucl. Mater. 196–198 (1992) 258] are compared with 2D toroidal images of CII and CIII radiation near the external divertor plates in TdeV ohmic plasmas ($I_p = 170$ kA, $n_e = 3\times10^{19}$ m^{-3}, $B_T = 1.4T$). The main plasma parameters in the SOL and divertor are calculated by the onion skin model (OSM) [K. Shimizu et al., J. Nucl. Mater. 196–198 (1992) 476] included in DIVIMP, the neutrals being calculated by EIRENE [D. Reiter, Internal Report, KFA, Julich, 1947 (1984), 2599 (1992)] in an iterative loop. The results show that the carbon is mainly created by chemical sputtering, with a considerable fraction coming from the external oblique plate. By interpreting experimental CII and CIII distributions, it is found that carbon is affected by the biasing (−125 to +125 V) through a combination of at least three processes: the ion flux to the plates, the $E \times B$ drift velocity, and the cross field diffusion.

1. Introduction

Biasing on TdeV ($R_{maj} = 0.86$ m, $a_{min} = 0.25$ m) consists of applying an electric potential between the horizontal divertor plates (both internal and external) while the wall and external oblique plate, are kept at ground potential (Fig. 1). Experimental and simulated 2D images of CII (514.5 nm, multiplet), CIII (464.7 nm, triplet) and D_α lines in the divertor region are compared during biasing. The diagnostic's toroidal view and high spatial resolution gives the opportunity to study local effects near the divertor horizontal and oblique plates. These line emissivities increase (decrease) with negative (positive) biasing by a factor of 2–3. The analyses using the OSM/EIRENE code coupled to DIVIMP are self consistent since both the D_α (background plasma) and the carbon are simulated simultaneously [1,3]. Although biasing is not practical on a reactor size tokamak, it is nonetheless a tool for better understanding the physics of the divertor plasma: recently TdeV's H-mode threshold was modified by biasinag [4].

2. Experimental results

The experimental set up of TdeV cameras is briefly described here, since the details were reported in a previous paper [5]. The 2D images are obtained using charge injection device cameras equipped with interference filters, and mounted on a rotatable periscope. The

☆ This paper was presented at the 13th International Conference on Plasma–Surface Interactions in Controlled Fusion Devices, San Diego, California, USA, 18–22, May 1998.

* Corresponding author. Tel.: +1-514 652 8709; fax: +1-514 652 8625.

E-mail address: haddad@ccfm.ireq.ca (E. Haddad).

0022-3115/00/$ - see front matter
PII: S0022-3115(99)00215-9

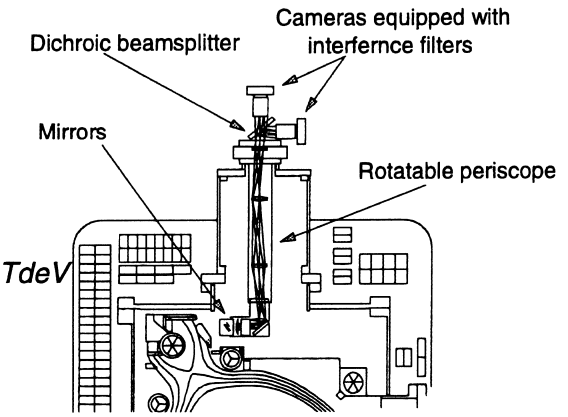

Fig. 1. Schematic of the divertor spectroscopic imaging diagnostic.

periscope's entrance pupil looks toroidally through a gap between two oblique plates giving toroidal images. The imaging system is absolutely calibrated. The plasma poloidal section imaged is approximately 100 mm × 100 mm with a relative spatial resolution of ~0.5 mm and an absolute resolution of ~ 2 mm. Fig. 2 shows the effect of biasing on the peak brightness of CII, CIII and D_α along the vertical axis Z, and a radial profile of CIII at $Z = 0.425$ m (between the oblique and horizontal plate). The $E \times B$ drift direction indicates the active plate: in negative biasing it is directed towards the external plate. During positive biasing, CII, CIII and D_α brightness decrease slightly near the horizontal plate remaining almost the same everywhere else. In negative biasing, the CII and D_α evolve similarly whereas the effect on CIII is localized mainly near the horizontal plate. Although the CIII emissivity increases (decreases) by a factor ~2–3 with negative (positive) biasing, we note that the normalized radial profiles (Fig. 2(c)) keep almost the same shape. As measured by the plate probes, the electron density increases (decreases) by a factor ~2 with negative (positive) biasing whereas the temperature stays almost the same within the experimental uncertainties (±20%). This increase of the flux towards the active plate is confirmed by the total deposited power on the horizontal plates, as measured by thermocouples, and by the pressure measurements in the divertor chamber. The fact that the effects of negative and positive biasing are not symmetrical suggests that the effect of biasing is more than a simple $E \times B$ effect.

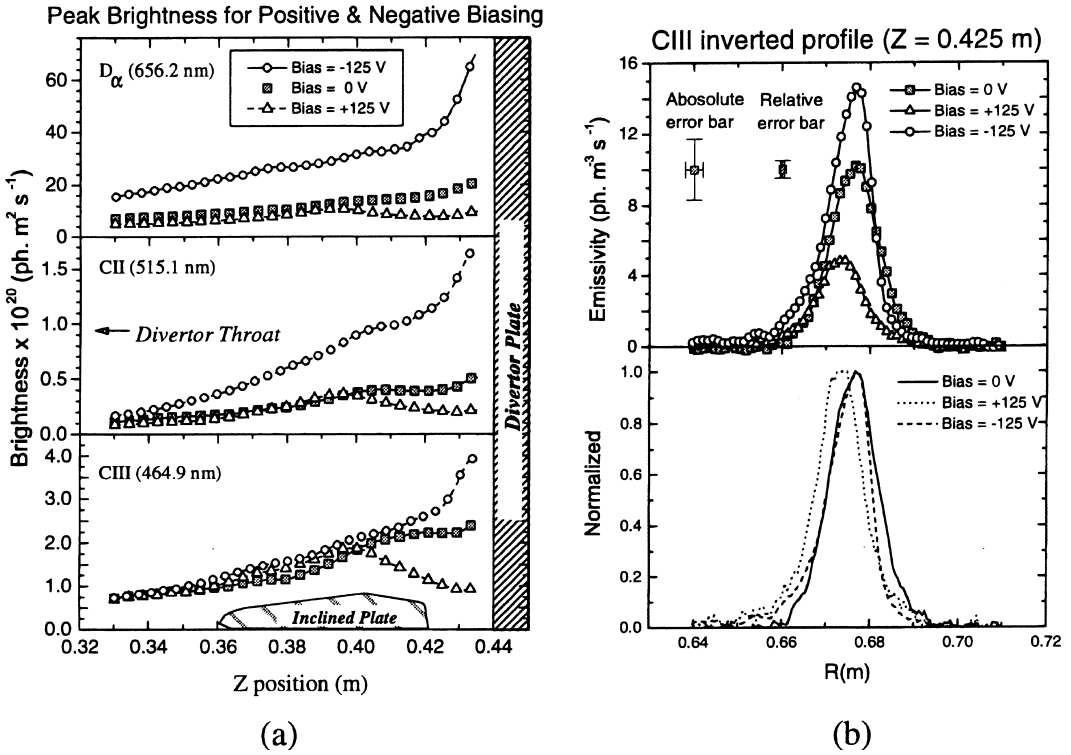

Fig. 2. Experimental results showing the effects of biasing on the spatial distribution of different radiating species in the divertor: (a) D_α, CII, and CIII peak brightness as a function of the Z positions. (b) Abel inverted profiles of the CIII emissivity 5 mm from the plate (top) and the same profiles normalized (bottom).

3. Simulations

3.1. DIVIMP/OSM/EIRENE

DIVIMP is a 2D Monte Carlo code which follows the trajectories of individual impurity particles in the edge plasma from their creation until their deposition on the divertor plates or wall, through all the ionization and recombination steps. Fluid models cannot always be applied accurately to the impurity transport in the SOL and divertor plasmas. The ionization time for low ionization species may be shorter than or of the same magnitude as their collision and thermalization times; and the ionization or collisional mean free path can be of the same order of magnitude as the geometrical scale length in the divertor [6]. The Monte Carlo approach is more flexible for treating various collisional effects or modelling impurity generation and the interactions between impurity and divertor plates or walls. DIVIMP main inputs are: the plasma geometry, the plasma background parameters as obtained from the OSM model, the sputtering model (physical, chemical, etc.) and the impurity cross-field diffusion. The main outputs are the density of impurity species in each cell, and the spectral line intensities. The atomic data are obtained from the ADAS [7] collisional radiative model.

Convergent and fast solutions of divertor plasma parameters of JT-60 [2] and JET [8], were successfully obtained from the OSM model. Taking the measured plasma parameters at the plates as initial conditions, it solves simultaneously the three fluid equations for conservation of particles, parallel momentum and energy in 1D along each flux tube. The OSM assumes that parallel transport dominates diffusion accross magnetic field lines, this latter being implicitely included in the model. The source/sink terms in each of the three equations is due to the interaction with recycled neutrals, which are simulated in an iterative loop with EIRENE, using the plasma parameters as calculated by the OSM model.

3.2. Image simulations

Inverting the toroidally integrated experimental images into poloidal emissivities to compare them with DIVIMP results, proved to be difficult to achieve in TdeV closed divertor, due to some mathematical instabilities in matrices inversion [5]. Instead we integrate simulated data along toroidal lines of sight

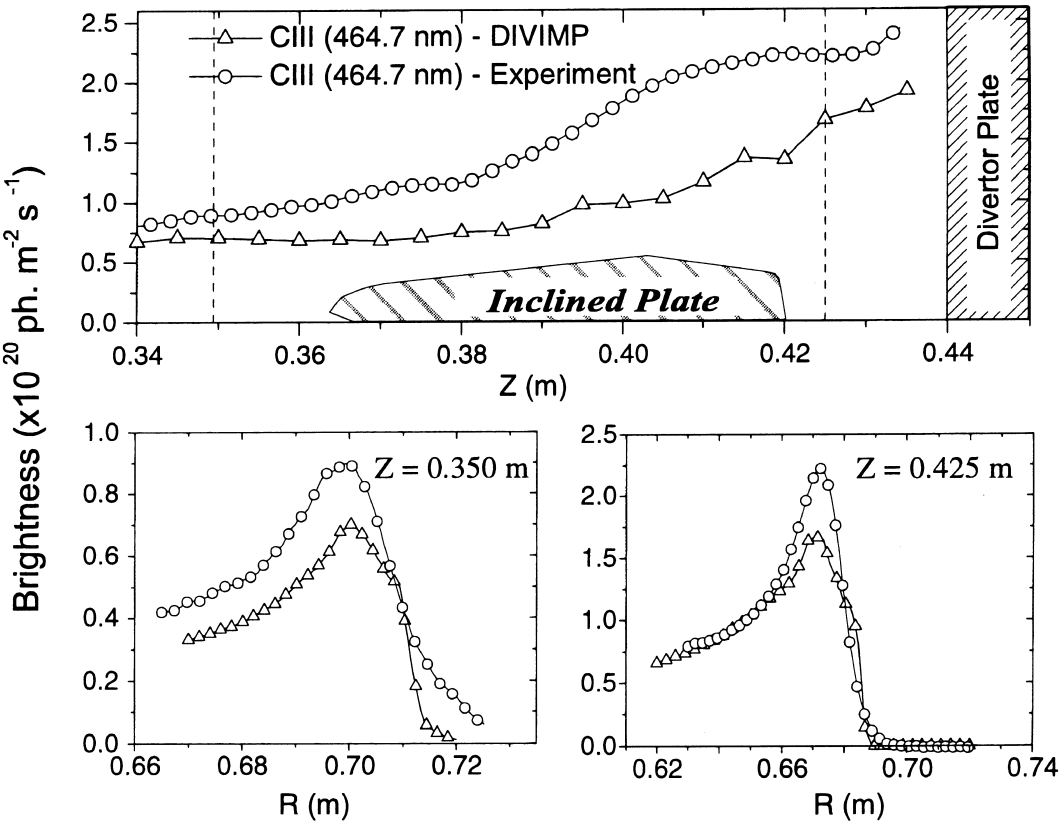

Fig. 3. Comparison between the experimental and simulated CIII: (top) The peak brightness along Z, (bottom) radial profiles (taken at dotted lines).

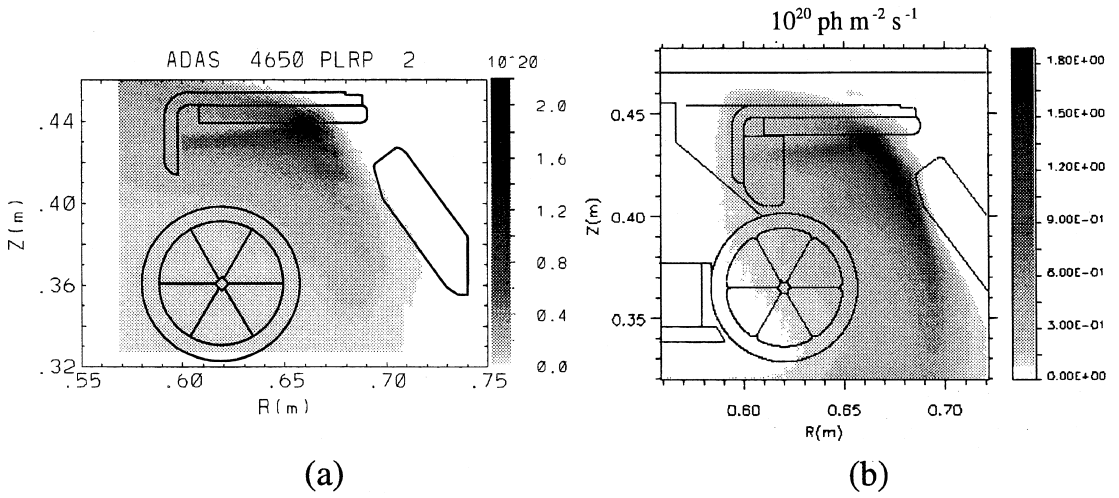

Fig. 4. Comparison between the convoluted DIVIMP results (a) and the experimental measurement (b) of CIII radiation.

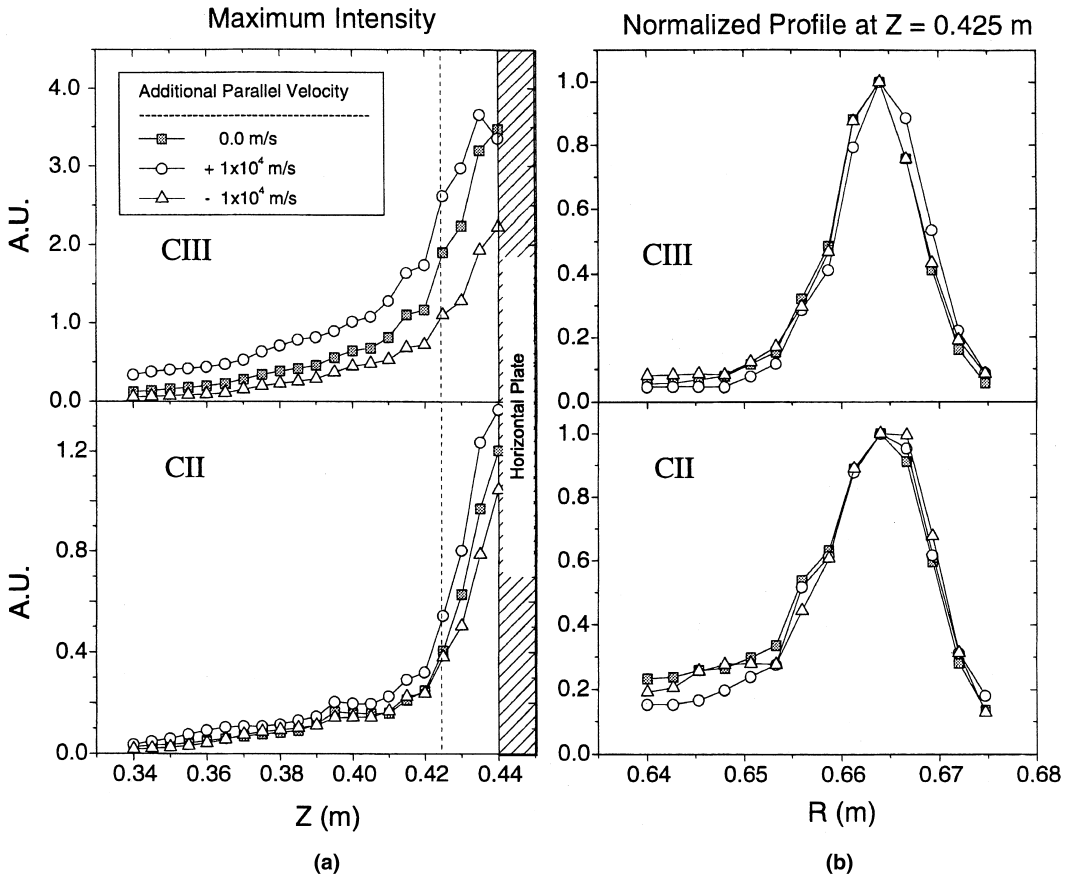

Fig. 5. DIVIMP results: Effect of an additional parallel velocity of the CII and CIII maximum peak intensity (a), and the normalized radial profile at $Z = 0.425$ m (b).

corresponding to the viewing configuration of the cameras, and compare them with experimental images. An array of lines are traced from the camera, through the knots of an unstructured triangular mesh, fixed on the camera object plane. Toroidal surfaces are simulated by rotating each DIVIMP cell in the divertor region, around the machine axis. As shown in Figs. 3 and 4, the 2D images permit semi-quantitative comparison such as the maximum emissivity, its spatial location, width, and the poloidal distribution along a specific ring.

4. Results and discussion

4.1. Sputtering yield

The physical sputtering yield of carbon from the two main data bases for fusion devices [9,10] agree within 15% for $T_i \geqslant 10$ eV (threshold of 33 eV for D^+). For $T_i \leqslant 8$ eV the sputtering yield decreases sharply, and an order of magnitude can be found between the two models. The physical sputtering yield of carbon from B_4C (created by wall boronization) bombarded by D^+ [11] is higher than that of graphite, but is still too low to explain the carbon radiation. Although the chemical sputtering is given by empirical formulas [12,13] and models can disagree on the contribution of a detailed chemical reaction, the total chemical yields, summed over all the chemical reactions, are of the same magnitude (1–2% for $T_i \geqslant 20$ eV). As suggested by experimental results from JET [15], we take a general multiplier factor of 0.3, assuming that the major part (70%) of chemically eroded carbon is redeposited on the plate surface after the breaking up of the hydrocarbon molecule. The sputtering yield modelling is acceptable, since for low T_i only chemical sputtering is important and for higher T_i physical sputtering becomes dominant hence the yields from data bases are in agreement.

4.2. The external oblique plate

The 2D images of CII and CIII show a tail of emissivity along the oblique plate. Although one could think to neglect this plate since it receives the lowest fluxes from

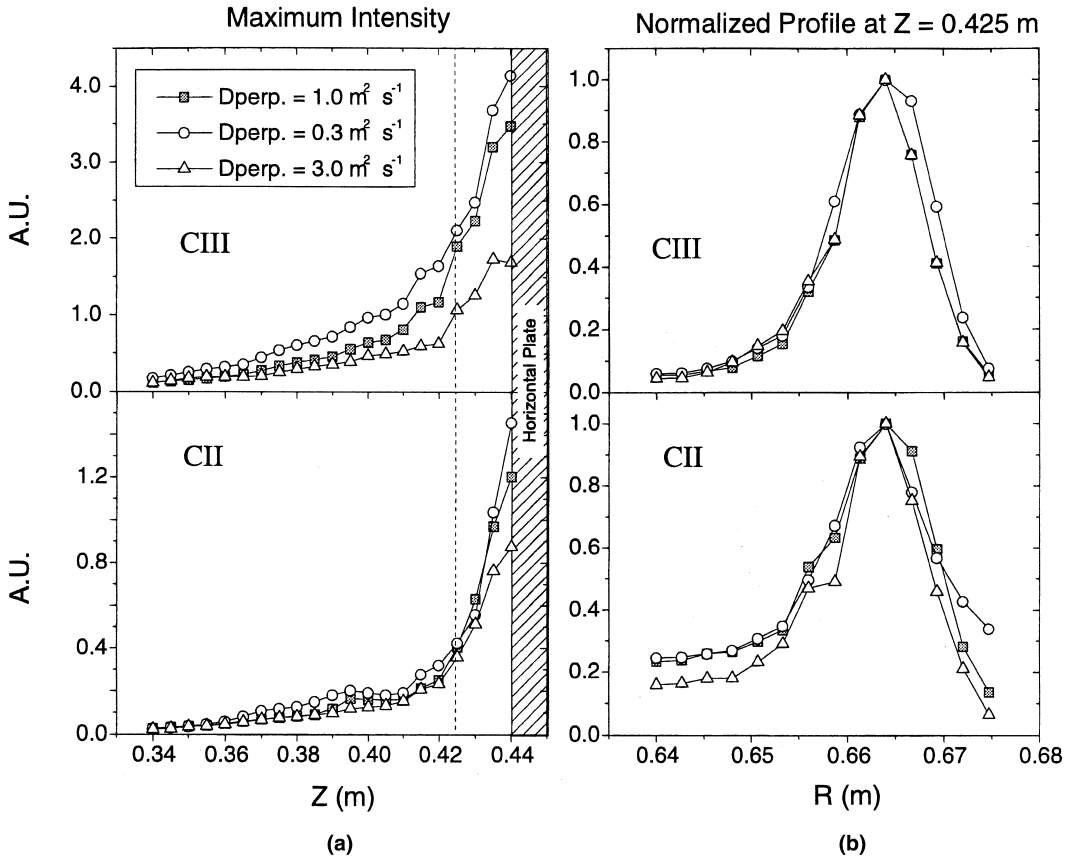

Fig. 6. DIVIMP results: Effect of the cross-field diffusivity on the CII and CIII maximum peak intensity (a) and the normalized radial profile at $Z = 0.425$ m (b).

the most external part of the SOL, it showed important effects. As measured by the thermocouples, the horizontal and oblique plate have similar amount of deposited power load (22 and 31 kJ, respectively) and with negative biasing they increase by the same ratio (to 30 and 40 kJ), although the oblique plate is kept at ground potential. We tried to check these effects either by reducing artificially the T_e, T_i, n_e, n_i profiles at this plate by a factor of 10, or by moving it back from the geometrical grid, keeping only the horizontal plate. Not only did the emissivity tail disappear, but also the total carbon level decreased by a factor of ~3, and we could not substitute its effect by increasing or decreasing other parameters such as the cross field diffusivity within realistic limits.

4.3. Biasing

The effects of the evolution of three processes with biasing are examined: the sputtering yield, the drift velocity and the cross-field diffusion. Since the biasing increases the ion velocity towards the active plate (negative biasing), we assume that the physical sputtering yield from the plate should increase. However, the CII and D_α are similarly affected by the biasing (Fig. 2(a)), and the ratio of CII/D_α stays almost the same, indicating that the sputtering yield did not vary largely with biasing. This is consistent with the probes measuring no large effect of biasing on the temperature in the divertor (<20%). But on the other hand the probes measure an increase (decrease) of the influx by a factor 1.5–3 on the outer plate with negative (positive) biasing. This can explain the evolution of carbon line emissivities, proportional to $\sim n_e^2$, the sputtering being proportional to $n_D^+ \sim n_e$. This is also in agreement with the total power deposited on the plates. We ote that in the main plasma, the CIV (154.8 nm) changes slightly and inversely to that of CII and CIII in the divertor region: it decreases (increases) by ~20% with negative (positive) biasing, whereas impurities created by physical sputtering increase the impurity level not only in the divertor but also in the main plasma [6].

A rough estimation of the drift effect is simulated by adding a parallel velocity $V_\parallel$ ($+10^4$ m/s, towards the horizontal plate) for negative biasing and (-10^4 m/s) for positive biasing, equivalent to the measured CIII velocity in the main plasma [14]. Fig. 5 shows a qualitative agreement of the variation of CIII peak brightness near the horizontal plate, between simulated and experimental data, whereas near the throat ($Z = 0.38$ m) the simulated data show higher effect than that observed. The CII simulated intensity does not seem to be very affected by the additional $V_\parallel$. Unfortunately we cannot go further in this analysis, since the simulated $V_\parallel$ is constant over all the SOL and is the same for all the carbon species.

The CIII peak emissivity along the Z axis is modified by biasing only near the horizontal plate, very differently from that of CII and D_α, suggesting a change of the cross-field diffusion with biasing; neutral and first ionization species have very short lifetimes and are less affected by the transport. Fig. 6 shows the effect of increasing or decreasing the diffusivity on simulated CII and CIII: a decrease (increase) of the diffusity will increase (decrease) the CIII intensity near the horizontal plate, whereas the CII is much less affected, suggesting a decrease of the diffusivity with negative biasing.

5. Conclusions

In TdeV, the carbon impurity in the divertor is mainly created by chemical sputtering, and the simulations show the importance of the external oblique plate in impurity production. Divertor plate biasing modifies the CII, CIII and D_α distribution by a complex way, changing the ion fluxes, the cross field transport, and the $E \times B$ drift.

Acknowledgements

The Centre canadien de fusion magnétique is supported by the Government of Canada, Hydro-Québec, and the Institut national de la recherche scientifique.

References

[1] P.C. Stangeby, J.D. Elder, J. Nucl. Mater. 196–198 (1992) 258.
[2] K. Shimizu et al., J. Nucl. Mater. 196–198 (1992) 476.
[3] D. Reiter, Internal report, KFA, Julich; 1947(1984), 2599 (1992).
[4] J.L. Lachambre et al., Profile modifications in TdeV during electron cyclotron heating, in: Presented at the 25th EPS Conference on Controlled Fusion and Plasma Physics, Prague, Czech Republic, June 1998.
[5] F. Meo et al., Rev. Sci. Instrum. 68 (1997) 3426.
[6] K. Shimizu et al., J. Nucl. Mater. 241–243 (1997) 167.
[7] H.P. Summers, Atomic Data and Analysis Structure, JET Internal Report, JET-IR (94)06.
[8] R. Monk et al., J. Nucl. Mater. 220–222 (1995) 612.
[9] W. Eckstein, J. Nucl. Mater. 248 (1997) 1, and references therein.
[10] Y.Yamamura, H. Tawara, Internal Report National Institute for Fusion Science, Nagoya, Japan, NIFS-DATA-23 1995.
[11] T. Ono, T. Kawamura, K. Ishii, Y. Yamamura, Internal Report National Institute for Fusion Science, Nagoya, Japan, NIFS-DATA-34, 1996.
[12] J. Roth, C. Garcia-Rosales, Nucl. Fusion 36 (1996) 1647.
[13] A.A. Haasz et al., J. Nucl. Mater. 248 (1997)19, and references therein.
[14] D. Lafrance et al., Phys. Plasmas 4 (1997) 3644.
[15] M Stamp et al., J. Nucl. Mater. 266–269 (1999) 685.